JACS
JOURNAL OF THE AMERICAN CHEMICAL SOCIETY

COMMUNICATION

pubs.acs.org/JACS

Monodisperse Porous $LiFePO_4$ Microspheres for a High Power Li-Ion Battery Cathode

Chunwen Sun, Shreyas Rajasekhara, John B. Goodenough,* and Feng Zhou

Texas Materials Institute, ETC 9.184, University of Texas at Austin, Austin, Texas 78712, United States

Supporting Information

ABSTRACT: A novel solvothermal approach combined with high-temperature calcinations was developed to synthesize on a large scale $LiFePO_4$ microspheres consisting of nanoplates or nanoparticles with an open three-dimensional (3D) porous microstructure. These micro/nanostructured $LiFePO_4$ microspheres have a high tap density and, as electrodes, show excellent rate capability and cycle stability.

In recent years, the ordered olivine lithium iron phosphate ($LiFePO_4$) has been extensively and intensively studied as a cathode material for power batteries in electric vehicles (EVs). Its advantages include a high theoretical specific capacity (170 mAh g^{-1}), low cost, environmental compatibility, and intrinsic thermal safety.[1] However, the rate performance of the original $LiFePO_4$ was significantly restricted by sluggish kinetics of electron and lithium-ion transport.[2] The rate performance and capacity of $LiFePO_4$ has been improved by coating with carbon or a metallic conducting layer,[3] by doping with isovalent ions,[4] or reducing the particle size.[5] Various methods have also been developed to prepare nanostructured $LiFePO_4$ particles, including hydrothermal/solvothermal,[6] sol−gel,[7] and hard-templating approaches.[8] Although the down-sizing strategy is effective for improving the performance of the electrode, it adversely affects the tap density and volumetric energy density. Generally, it is believed that microsized spherical particles can easily form close-packed arrays.[9] Therefore, $LiFePO_4$ microsphere powder with a micro/nanostructure is highly desired for designing high-performance lithium-ion batteries with high volumetric energy density and good rate capability. To our knowledge, there are no reports on three-dimensional (3D) $LiFePO_4$ architectures composed of nanoplates assembled to give a total particle size on the micrometer scale. Herein, we report a novel solvothermal approach combined with high-temperature calcinations of broad application to synthesize $LiFePO_4$ microspheres consisting of nanoplates or nanoparticles with an open 3D porous microstructure. Our results suggest an interesting approach for controlling the morphology of microspheres by tuning the complex chemistry for the nucleation and growth of crystals. In this study, conductive polypyrrole (PPy) was also deposited onto carbon-coated $LiFePO_4$ microspheres by a chemical polymerization process in an attempt to increase their rate capability as electrodes in a Li/$LiFePO_4$ half-cell.

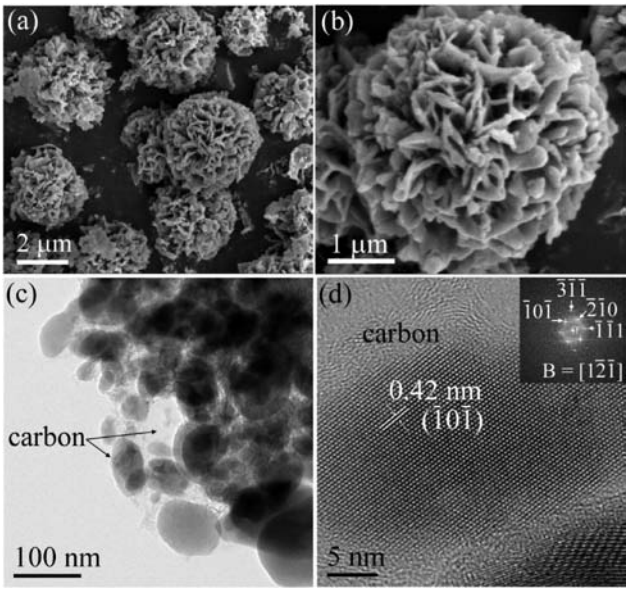

Figure 1. Representive SEM and TEM images of the flowerlike $LiFePO_4$ microspheres: (a) overall morphology of the products; (b) high-magnification SEM image of an individual microsphere, revealing the constituent details of the microsphere; (c) overview of an ensemble of nanoplates at the edge of a microsphere coated with carbon; (d) HRTEM image of a well-crystallized nanoplate (inset: the FFT pattern, B denotes the beam direction).

The phase purity and crystal structure of the products obtained were examined by XRD. Figure S1 (see Supporting Information [SI]) shows that the pattern of the calcined products can be indexed as orthorhombic $LiFePO_4$ (JCPDS No. 83-2092).

The size and morphology of the products were examined by scanning electron microscopy (SEM). Figure 1a shows that most of the $LiFePO_4$ sample consists of monodispersed spherical particles with flowerlike texture. The diameter of the microspheres is 1−3 μm. It can be clearly seen that these flowerlike microspheres are composed of many nanoplate petals with an average thickness of about 80 nm; these nanoplates interweave together forming an open porous structure (Figure 1b). Such a well-organized porous structure is expected to facilitate electrolyte penetration into the electrode particles, thus providing more interface area between the electrode material and the electrolyte.

The morphology and structure of the flowerlike $LiFePO_4$ hierarchical architectures were further characterized by transmission

Received: December 15, 2010
Published: January 26, 2011

dx.doi.org/10.1021/ja1110464 | J. Am. Chem. Soc. 2011, 133, 2132–2135

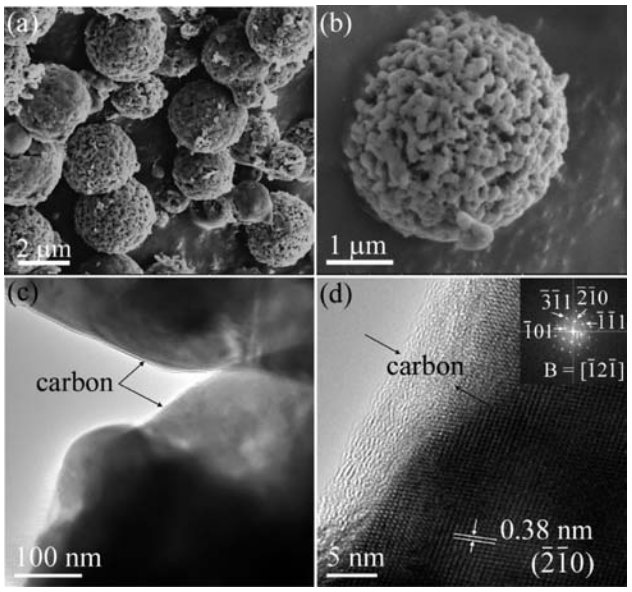

Figure 2. Representive SEM and TEM images of the walnut-shaped $LiFePO_4$ microspheres: (a) overall morphology of the products; (b) high-magnification SEM images of an individual microsphere; (c) overview of an ensemble of nanoparticles at the edge of a microsphere coated with carbon; (d) HRTEM image of a well-crystallized nanoparticle (inset: the FFT pattern, B denotes the beam direction).

electron microscopy (TEM) and high resolution TEM (HRTEM). A HRTEM image (Figure 1c) taken on an individual nanoplate of flowerlike $LiFePO_4$ microspheres displays clear crystal planes with a *d*-spacing of 0.42 nm, corresponding to the $(\bar{1}0\bar{1})$ planes of orthorhombic $LiFePO_4$. In addition, it is clearly seen from the HRTEM image that an amorphous carbon layer characterized by Raman spectra (Figure S4, SI) with a thickness of 2−3 nm covered the surface of the $LiFePO_4$ particles. The inset in Figure 1d is the indexed fast Fourier transform (FFT) pattern of Figure 1d, which also indicates the single crystal characteristics of the nanoplates. The lattice spacing of approximately 0.42 nm in real space in Figure 1d is comparable to the *d*-spacing determined by the analysis of inverse FFT for the reflection $[\bar{1}0\bar{1}]$ (Figure S3a, SI), thereby confirming the FFT pattern analysis.

Figure 2a shows a typical low-magnification SEM image of the $LiFePO_4$ sample synthesized in the absence of ethylenediamine. It can be clearly seen that most of the sample is monodisperse microspheres with walnut kernel morphology. The diameter of the microspheres is 2−5 μm. Figure 2b displays an individual microsphere composed of nanoparticles. A TEM image (Figure 2c) from the edge of these microspheres reveals that they have a relatively smooth and closed structure, covered with a carbon coating. A HRTEM image (Figure 2d) of this edge shows clear crystal planes with a *d*-spacing of 0.38 nm, corresponding to the $(\bar{2}\,\bar{1}0)$ planes of orthorhombic $LiFePO_4$.

Figure S5 (SI) shows the nitrogen adsorption−desorption isotherms and the corresponding Barret−Joyner−Halenda (BJH) pore size distribution curves of the obtained $LiFePO_4$ microspheres with two different morphologies. The adsorption isotherm for the walnut-shaped $LiFePO_4$ microspheres (hereafter abbreviated as WMS-$LiFePO_4$) is a type III curve, indicating a macroporous characteristic.[10] However, the adsorption isotherm for flowerlike $LiFePO_4$ microspheres (hereafter abbreviated as FMS-$LiFePO_4$) shows a type IV adsorption−desorption isotherm with H3-type hysteresis, a feature of mesoporous material.[10] The measured Brunauer−Emmett−Teller (BET) area for flowerlike and walnut-shaped $LiFePO_4$ microspheres are 32.9 and 3.6 $m^2\ g^{-1}$, respectively. The average pore diameters of FMS-$LiFePO_4$ is 3.8 nm, calculated from the desorption branch of the nitrogen isotherm with the BJH method. The corresponding BJH desorption cumulative pore volumes is 0.134 $cm^3\ g^{-1}$. For the WMS-$LiFePO_4$, the average pore diameters and the corresponding BJH desorption cumulative pore volumes are 1.94 nm and 0.015 $cm^3\ g^{-1}$, respectively.

At present, the battery for electric vehicles is still a big pack. The tap density of electrode materials is directly related to the volumetric energy density of a battery. The tap density of $LiFePO_4$ with nanoparticles and an irregular carbon coating is generally less than 1.0 g cm^{-3}. However, the tap densities of flowerlike and walnut-shaped microspheres can reach about 1.1 and 1.2 g cm^{-3}, respectively. This characteristic makes $LiFePO_4$ microsphere electrodes have a higher volumetric energy density. In addition, an Fe^{2+} salt has been employed as a starting material in most previous hydrothermal and other synthetic routes,[6b,11] which is expensive and easily oxidized as compared to the low-cost Fe^{3+}-salt alternative. Therefore, additional reducing agents (ascorbic acid, citric acid, or alcohols) and/or an inert gas atmosphere are always used in these syntheses to prohibit the oxidation of Fe^{2+} to Fe^{3+} during the synthesis process of $LiFePO_4$.

In this work, our strategies are to control the morphology of $LiFePO_4$ particles by means of the reducing and complex characteristics of ethylene glycol[12] (EG) and the stronger complexing ability of ethylenediamine.[13] The EG medium can act not only as a solvent in the process, but also as a stabilizer to limit the particle growth and prevent the agglomeration due to the chelates of EG.[5b,14] In this synthesis, EG reduces Fe^{3+} ions into Fe^{2+} ions in the liquid solution. The products after the solvothermal reaction mainly consist of $Fe_3(PO_4)_2(H_2O)_2$ and Li_3PO_4 phases for FMS-$LiFePO_4$ (Figure S6a [SI]), and $Fe_3(PO_4)_2(OH)_2$ and Li_3PO_4 for WMS-$LiFePO_4$ (Figure S6b [SI]), respectively.

As a cosolvent, the presence of ethylenediamine is a critical condition for the formation of hierarchically flowerlike $LiFePO_4$ microspheres. Microspheres consisting of nanoparticles, instead of nanoplates, were formed where ethylenediamine was absent (see a and b of Figure 2). Previous studies have demonstrated that ethylenediamine has a stronger chelating ability for some transition-metal ions.[12] Therefore, ethylenediamine has a great effect on the release of isolated iron ions in this synthetic system, which influences the crystal growth.

On the basis of the above experimental evidence, the formation of $LiFePO_4$ microspheres seems to follow the scheme proposed by LaMer *et al.*[15] The precursors are solute complexes that lead to the solid phase by reduction and hydrolysis. The formation of the solid phase proceeds through two separate steps, a very short nucleation step followed by a particle growth step kinetically controlled either by the chemical reaction itself or by diffusion of the reacting species toward the interface. The primary particles, grown initially, aggregate into uniform larger monodispersed spherical particles with a size on the micrometer scale. This aggregation process has been reported to be the rule in the particle formation of various monodispersed oxides.[16] As for the case of flowerlike microspheres, the primary particles may first aggregate into nanoplates due to the controlled release of

dx.doi.org/10.1021/ja1110464 |*J. Am. Chem. Soc.* 2011, 133, 2132–2135

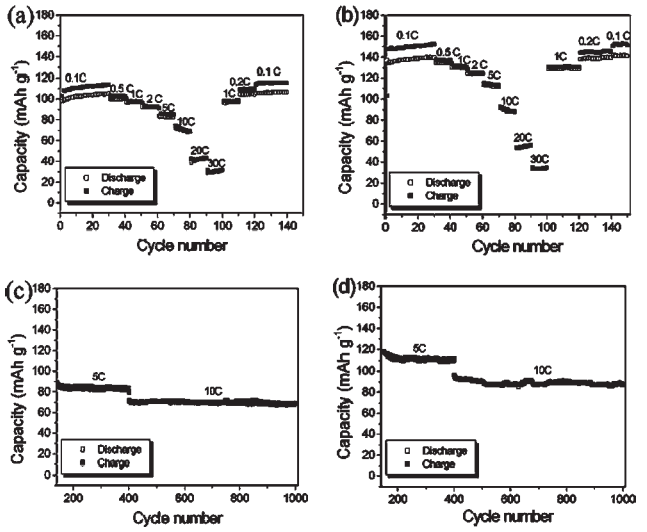

Figure 3. The charge/discharge capacities at different current rates and cycling performances of the FMS-$LiFePO_4$/C (a, c) and FMS-$LiFePO_4$/C/PPy (b, d).

isolated iron ions and then self-assemble into microspheres. The driving force for the colloid particle reorganization corresponds to a reduction in surface free energy.[17] Therefore, the overall shape of the resultant products is typically spherical.

In order to examine the potential application of FMS-$LiFePO_4$ in high-power Li-ion batteries, the electrochemical properties of $LiFePO_4$ microspheres were tested in 2032-type coin half-cells at 298 K. The rate performance comparison of FMS-$LiFePO_4$/C and FMS-$LiFePO_4$/C/PPy is shown in a and c of Figure 3. Compared with that of FMS-$LiFePO_4$/C, the specific capacity of FMS-$LiFePO_4$/C-based composite cathodes with PPy is greatly enhanced at rates from 0.1C to 30C, especially at lower current rates. The FMS-$LiFePO_4$/C/PPy composite exhibits a discharge capacity of 140 mAh g^{-1} at 0.1 C charge/discharge rate. The reversible specific capacity of FMS-$LiFePO_4$/C/PPy remains approximately 110 mAh g^{-1} at 5C charge/discharge rate and 86 mAh g^{-1} at 10C charge/discharge rate for a total of 1000 cycles. Although the FMS-$LiFePO_4$/C initially has a slightly reduced discharge specific capacity, it shows good cycle stability (Figure 3c). This can be attributed to its well-crystallized nanoparticles and the structural robustness of the flowerlike microspheres. The rate performance of FMS-$LiFePO_4$/C/PPy is almost equal to those of $LiFePO_4$ microspheres with double carbon coating[9c] and nanoporous $LiFePO_4$ microspheres[18a] recently reported by Sun *et al.* at the rate of 0.1C-10C (Figure S8 [SI]), while it is better than those of the solid $LiFePO_4$ microspheres reported by Xie *et al*,[9a] the porous $LiFePO_4$/C microspheres synthesized by Yu *et al.* using a sol−gel method,[18b] and hollow spheres reported by Lee *et al.*[18c] The electrochemical performances of WMS-$LiFePO_4$/C and WMS-$LiFePO_4$/C/PPy are shown in Figures S9−S13 (SI). At low rates, both FMS-$LiFePO_4$/C/PPy and WMS-$LiFePO_4$/C/PPy samples exhibit comparable performance. However, at higher rates, the superior behavior of the FMS-$LiFePO_4$ is revealed.

The remarkable advantage of the FMS-$LiFePO_4$/C/PPy materials is their retention of an excellent rate capability and cyclability with an improved volumetric energy density. These excellent rate and cycling performances may be the result of the following: (a) a fast reaction and ionic diffusion kinetics of nanosized particles of C-$LiFePO_4$; (b) good electronic contact by retaining the ability to coat individual nanoparticles with carbon and the conductive PPy; (c) the well-crystallized nanoparticles and the structural robustness of $LiFePO_4$ microspheres. The electrochemical performance of $LiFePO_4$ microspheres might be further improved by optimizing the carbon structure with an increased amount of sp^2-type carbon.[9a,9b]

In summary, we have developed a two-step process for preparing porous $LiFePO_4$ microspheres with well-defined flowerlike or walnut-shaped morphologies on a large scale. This flowerlike morphology provides interconnected open pores that allow carbon coating and electrolyte penetration, improving the electronic conductivity and reducing the diffusion path of the lithium ions. This feature, combined with the high tap density, results in electrodes having a high volumetric energy density and excellent rate capability. This novel method can be extended to obtain various monodisperse porous materials (e.g., $LiMnPO_4$) for use in energy storage and conversion, as well as catalysis.

■ ASSOCIATED CONTENT

Supporting Information. XRD pattern, SEM images, nitrogen adsorption and desorption isotherms, charge/discharge curves at various current rates, and Raman spectra as well as experimental details. This material is available free of charge via the Internet at http://pubs.acs.org.

■ AUTHOR INFORMATION

Corresponding Author
jgoodenough@mail.utexas.edu

■ ACKNOWLEDGMENT

Financial support from the Energy Frontier Research Center (EFRC) of DOE, United States, is acknowledged (Grant DE-SC0001091). We thank Dr. Jing Wu for help with Raman spectra measurement.

■ REFERENCES

(1) (a) Aricò, A. S.; Bruce, P..; Scrosati, B.; Tarascon, J. M.; Schalkwijik, W. V. *Nat. Mater.* **2005**, *4*, 366–377. (b) Tarascon, J. M.; Armand, M. *Nature* **2001**, *414*, 359–496. (c) Armand, M.; Tarascon, J. M. *Nature* **2008**, *451*, 652–657. (d) Gibot, P.; Casas-Cabanas, M.; Laffont, L.; Levasseur, S.; Carlach, P.; Hamelet, S.; Tarascon, J. M.; Masquelier, C. *Nat. Mater.* **2008**, *7*, 741–747.

(2) Padhi, A.; Nanjundaswamy, K.; Goodenough, J. B. *J. Electrochem. Soc.* **1997**, *144*, 1188–1194. (b) Padhi, A.; Nanjundaswamy, K.; Okada, S.; Goodenough, J. B. *J. Electrochem. Soc.* **1997**, *144*, 1609–1613.

(3) (a) Ravet, N.; Goodenough, J. B.; Besner, S. Simoneau, M.; Hovington, P.; Armand, M. *196th Electrochemical Society Meeting*, Honolulu, HI, 1999; Electrochemical Society: Pennington, NJ, 1999; Abstract 127. (b) Huang, H.; Yin, S. C.; Nazar, L. F. *Electrochem. Solid-State Lett.* **2001**, *4*, A170–A172.

(4) (a) Wang, D. Y.; Li, H.; Shi, S. Q.; Huang, X. J.; Chen, l.Q. *Electrochim. Acta* **2005**, *50*, 2955–2958. (b) Chung, S. Y.; Bloking, J. T.; Chiang, Y. M. *Nat. Mater.* **2002**, *1*, 123–128.

(5) (a) Delacourt, C.; Poizot, P.; Levasseur, S.; Masquelier, C. *Electrochem. Solid-State Lett.* **2006**, *9*, A352–255. (b) Kim, D. H.; Kim, J. *Electrochem. Solid-State Lett.* **2006**, *9*, A439–A442.

(6) (a) Chen, J.; Wang, S.; Whittingham, M. S. *J. Power Sources* **2007**, *174*, 442–448. (b) Ellis, B.; Kan, W. H.; Makahnouk, W. R. M.; Nazar, L. F. *J. Mater. Chem.* **2007**, *17*, 3248–3254.

(7) (a) Choi, D.; Kumta, P. N. *J. Power Sources* **2007**, *163*, 1064–1069. (b) Dominko, R.; Bele, M.; Goupil, J. M.; Gaberscek, M.; Hanzel, D.; Arcon, I.; Jamnik *J. Chem. Mater.* **2007**, *19*, 2960–2969. (c) Hsu, K.; Tsay, S.; Hwang, B. *J. Mater. Chem.* **2004**, *14*, 2690–2695. (c) Yang, J.; Xu, J. *Electrochem. Solid-State Lett.* **2004**, *7*, A515–A518.

(8) Lim, S.; Yoon, C. S.; Cho, J. *Chem. Mater.* **2008**, *20*, 4560–4564.

(9) (a) Xie, H. M.; Wang, R. S.; Ying, J. R.; Zhang, L. Y.; Jalbout, A. F.; Yu, H. Y.; Yang, G. L.; Pan, X. M.; Su, Z. M. *Adv. Mater.* **2006**, *18*, 2609–2613. (b) Sun, L.; Li, M.; Cui, R.; Xie, H.; Wang, R. *J. Phys. Chem.. C* **2010**, *114*, 3297–3303. (c) Oh, S. W.; Myung, S.; Oh, S. M.; Oh, K. H.; Amine, K.; Scrosati, B.; Sun, Y. K. *Adv. Mater.* **2010**, *22*, 4842–4845. (d) Qian, J.; Zhou, M.; Cao, Y.; Ai, X.; Yang, H. *J. Phys. Chem. C* **2010**, *114*, 3477–3482.

(10) Sing, K.; Everett, D.; Haul, R.; Moscou, L.; Pierotti, R. A.; Rouquérol, J.; Siemieniewska, T. *Pure Appl. Chem.* **1985**, *57*, 603–619.

(11) (a) Yang, H.; Wu, X.; Cao, M.; Guo, Y. *J. Phys. Chem. C* **2009**, *113*, 3345–3351. (b) Dokko, K.; Koizumi, S.; Nakano, H.; Kanamura, K. *J. Mater. Chem.* **2007**, *17*, 4803–4810.

(12) (a) Poul, L.; Ammar, S.; Jouini, N.; Fievet, F.; Villain, F. *Solid State Sci.* **2001**, *3*, 31–42. (b) Larcher, D.; Patrice, R. *J. Solid State Chem.* **2000**, *154*, 405–411.

(13) (a) Sun, C.; Li, H.; Zhang, H.; Wang, Z.; Chen, L. *Nanotechnology* **2005**, *16*, 1454–1463. (b) Yin, L.; Wang, Y.; Pang, G.; Koltypin, Y.; Gedanken, A. *J. Colloid Interface Sci.* **2002**, *246*, 78–84.

(14) Qiu, L.; Pol, V. G.; Calderon-Moreno, J.; Gedanken, A. *Ultrason. Sonochem.* **2005**, *12*, 243–247.

(15) Lamer, V. K.; Dinegar, R. H. *J. Am. Chem. Soc.* **1950**, *72*, 4847–4854.

(16) Ocana, M.; Rodriguez-Clemente, R.; Serna, C. J. *Adv. Mater.* **1995**, *7*, 212–216.

(17) Sun, C.; Sun, J.; Xiao, G.; Zhang, H.; Qiu, X.; Li, H.; Chen, L. *J. Phys. Chem. B* **2006**, *110*, 13445–13452.

(18) (a) Oh, S. W.; Myung, S. T.; Bang, H. J.; Yoon, C. S.; Amine, K.; Sun, Y. K. *Electrochem. Solid-State Lett.* **2009**, *12*, A181–A185. (b) Yu, F.; Zhang, J.; Yang, Y.; Song, G. *J. Mater. Chem.* **2009**, *19*, 9121–9125. (c) Lee, M.; Kim, J.; Song, H. *Chem. Commun.* **2010**, *46*, 6795–6797.